The GFDL Hurricane Prediction System and Its Performance in the 1995 Hurricane Season

YOSHIO KURIHARA, ROBERT E. TULEYA, AND MORRIS A. BENDER

Geophysical Fluid Dynamics Laboratory/NOAA, Princeton University, Princeton, New Jersey

ABSTRACT

The Geophysical Fluid Dynamics Laboratory (GFDL) Hurricane Prediction System was adopted by the U.S. National Weather Service as an operational hurricane prediction model in the 1995 hurricane season. The framework of the prediction model is described with emphasis on its unique features. The model uses a multiply nested movable mesh system to depict the interior structure of tropical cyclones. For cumulus parameterization, a soft moist convective adjustment scheme is used. The model initial condition is defined through a method of vortex replacement. It involves generation of a realistic hurricane vortex by a scheme of controlled spinup. Time integration of the model is carried out by a two-step iterative method that has a characteristic of frequency-selective damping.

The outline of the prediction system is presented and the system performance in the 1995 hurricane season is briefly summarized. Both in the Atlantic and the eastern Pacific, the average track forecast errors are substantially reduced by the GFDL model, compared with forecasts by other models, particularly for the forecast periods beyond 36 h. Forecasts of Hurricane Luis and Hurricane Marilyn were especially skillful. A forecast bias is noticed in cases of Hurricane Opal and other storms in the Gulf of Mexico. The importance of accurate initial conditions, in both the environmental flow and the storm structure, is argued.

1. Introduction

In the 1995 hurricane season, the GFDL (Geophysical Fluid Dynamics Laboratory) Hurricane Prediction System was adopted by the U.S. NWS (National Weather Service) as an operational hurricane forecast model. The purpose of this paper is to describe the structure of the hurricane model, with emphasis on its unique features, and to present an overall picture of the prediction system. Also, the system performance in the 1995 hurricane season is summarized.

The dynamical model used in the prediction system is an outgrowth of a research model, the construction of which began in 1970 at GFDL/NOAA (National Oceanic and Atmospheric Administration). The research model has been used in a number of idealized numerical experiments and produced results that demonstrated a high degree of simulation capability. Being encouraged with the performance of the research model, we anticipated a substantial potential benefit from application of the model to forecasting real tropical cyclones.

The work to convert the research model to a comprehensive prediction system started in the mid-1980s.

The prediction capability of the GFDL hurricane model was first investigated using global analysis data of the National Centers for Environmental Prediction (NCEP) for cases of Hurricane Gloria 1985 (Kurihara et al. 1990). The obtained results, which were quite promising, indicated that a prediction system had to include a model initialization process, in addition to a process to link the model with the database obtained from high quality analysis (Kanamitsu 1989; Kanamitsu et al. 1991; Lord 1991; Parrish and Derber 1992). The system was nearly complete by 1992, when it was successfully applied to several storms including Hurricane Andrew in the Atlantic and Iniki in the Pacific. In 1993, the model showed substantial improvement over the available operational track guidance, notably by successfully forecasting the sharp recurving of Hurricane Emily near the North Carolina Outer Banks. The model was transferred to NCEP in 1994 for a parallel mode test. Intensive effort was made in this step to improve throughput efficiency so that the system would meet a demand that the entire procedure for making a 72-h prediction be completed in less than 20 min. The power of the current generation of supercomputing was indispensable to this end. Prompted by the skill demonstrated by the system in the 1994 season, the NWS officially adopted the GFDL system in 1995 for use as a guidance tool for hurricane prediction.

The equations governing the hurricane model are presented in section 2. The fundamentals of numerical mod-

Corresponding author address: Dr. Yoshio Kurihara, Geophysical Fluid Dynamics Laboratory, Princeton University, Forrestal Campus, U.S. Route 1, P.O. Box 308, Princeton, NJ 08542.
E-mail: yk@gfdl.gov

eling of a weather system are 1) to use sufficiently high resolution to resolve the primary structure of the system, 2) to incorporate accurate model physics that drives the system, 3) to provide the model with a set of consistent initial conditions, and 4) to run a model with little computational noise. How we attempt to achieve these objectives in the GFDL hurricane model is explained in section 3 (how hurricanes are portrayed in the model), section 4 (how various processes are parameterized), section 5 (how hurricanes are represented in the initial condition), and section 6 (how the model is time integrated), respectively. In section 7, the prediction system and its performance in the 1995 hurricane season are briefly summarized. Remarks on further improvement of the system are presented in section 8.

2. Governing equations

The primitive equations expressed in spherical coordinates λ (longitude), φ (latitude), and σ (pressure normalized by the surface value) are used in the GFDL hurricane model to describe the time tendency ($\partial/\partial t$) of u (zonal component of the wind), v (meridional component of the wind), T (temperature), r (mixing ratio of the water vapor), and p_* (surface pressure). In addition, an equation for T_* (land surface temperature) is used in the model.

They are written with the use of an operator $D(h)$ (h represents a variable, u, v, T, or r):

$$D(h) = \frac{\partial p_* uh}{\alpha \partial \lambda} + \frac{\partial p_* vh \cos\varphi}{\alpha \partial \varphi} + \frac{\partial p_* \dot\sigma h}{\partial \sigma},$$

where $\dot\sigma$ denotes the vertical σ velocity ($d\sigma/dt$) and $\alpha = a \cos\varphi$ (a is the radius of the earth).

Equation of motion

$$\frac{\partial p_* u}{\partial t} = -D(u) + \left(f + \frac{\tan\varphi}{a} u \right) p_* v$$
$$- p_* \frac{\partial \Phi_p}{\alpha \partial \lambda} + {}_H F_\lambda + {}_V F_\lambda$$

$$\frac{\partial p_* v}{\partial t} = -D(v) - \left(f + \frac{\tan\varphi}{a} u \right) p_* u$$
$$- p_* \frac{\partial \Phi_p}{\alpha \partial \varphi} + {}_H F_\varphi + {}_V F_\varphi.$$

Here f is the Coriolis parameter, Φ_p is the geopotential of an isobaric surface, and $({}_H F_\lambda, {}_H F_\varphi)$ and $({}_V F_\lambda, {}_V F_\varphi)$ are the frictional effects due to the horizontal and vertical diffusion of the momentum, respectively. Note that the pressure gradient force is determined from the slope of an isobaric surface. This form is used as it can avoid a truncation error that exists in the often used two-term form (see appendix A).

Thermodynamical equation

$$\frac{\partial p_* T}{\partial t} = -D(T) + \frac{R}{C_p} \frac{T\omega}{\sigma} + {}_H F_T + {}_V F_T$$
$$+ \text{QCON} + \text{TRAD}.$$

Here R is the gas constant, C_p specific heat at constant pressure, ω the vertical p velocity, ${}_H F_T$ and ${}_V F_T$ the effect of horizontal and vertical diffusion, QCON and TRAD the tendencies related to the condensation process and radiation, respectively.

Equation for the land surface temperature

$$\frac{\partial T_*}{\partial t} = \frac{-G}{\rho_s c_s d}.$$

Here G is the net upward heat flux at the ground surface, $\rho_s c_s$ is the soil heat capacity, and d is the damping depth.

Equation for the mixing ratio of water vapor

$$\frac{\partial p_* r}{\partial t} = -D(r) + {}_H F_r + {}_V F_r + \text{RCON}.$$

Here ${}_H F_r$ and ${}_V F_r$ represent the effect of horizontal and vertical diffusion, respectively, and RCON is the tendency related to the condensation process.

Surface pressure tendency equation

$$\frac{\partial p_*}{\partial t} = -\int_0^1 \left(\frac{\partial p_* u}{\alpha \partial \lambda} + \frac{\partial p_* v \cos\varphi}{\alpha \partial \varphi} \right) d\sigma.$$

Vertical sigma velocity

$$\dot\sigma = \frac{1}{p_*} \left[-\sigma \frac{\partial p_*}{\partial t} - \int_0^\sigma \left(\frac{\partial p_* u}{\alpha \partial \lambda} + \frac{\partial p_* v \cos\varphi}{\alpha \partial \varphi} \right) d\sigma \right].$$

Vertical p velocity

$$\omega = p_* \sigma \left[\frac{\dot\sigma}{\sigma} - \frac{\partial \dot\sigma}{\partial \sigma} - \left(\frac{\partial u}{\alpha \partial \lambda} + \frac{\partial v \cos\varphi}{\alpha \partial \varphi} \right) \right].$$

Hydrostatic relation

The geopotential of σ surface, Φ, is related to the temperature by

$$\frac{\partial \Phi}{\partial \ln\sigma} = -RT \quad \text{or} \quad \Phi - RT = \frac{\partial \Phi \sigma}{\partial \sigma}.$$

3. Grid configuration

a. High vertical resolution in the boundary layer

Since the evolution of tropical cyclones strongly depends on the processes at the underlying surface and in the planetary boundary layer over a large domain, relatively high vertical resolution is used in the planetary

Table 1. The σ levels and their approximate heights (m).

| Level k	σ	Height (m)
1	0.0207469	26 103
2	0.0739862	18 004
3	0.1244004	14 709
4	0.1745733	12 562
5	0.2246687	10 964
6	0.2747291	9660
7	0.3247711	8539
8	0.3748014	7550
9	0.4248250	6662
10	0.4974484	5516
11	0.5935378	4189
12	0.6881255	3044
13	0.7772229	2076
14	0.8563145	1289
15	0.9204018	694
16	0.9604809	339
17	0.9814907	157
18	0.9949968	42

Fig. 1. One example of the configuration of the triply nested meshes. Each dot represents a grid point at the center of a mesh. Mesh C shown is a part of its domain.

boundary layer. Table 1 shows the positions of sigma levels in the model. Variables are specified at these levels except that the vertical σ velocity is specified at half levels in between.

b. Multiply nested mesh

The GFDL hurricane model is a regional grid model. Currently, the model domain spans from 10°S to 65°N in the latitudinal direction and extends 75° in the longitudinal direction. The lateral boundary of the domain is determined from the initial position of the storm and the NHC (National Hurricane Center) forecast 72-h position, if available. It remains fixed during a forecast period and is open to receive the forecast information from a global model.

A sufficiently high horizontal resolution is required in order to resolve the interior structure of hurricanes. On the other hand, a coarser resolution is sufficient to represent the storm's outer region and the environment. Under the circumstances and from a standpoint of computational efficiency, a mesh nesting approach was taken (Kurihara et al. 1979; Kurihara and Bender 1980). Figure 1 shows the initial configuration of the triply nested meshes of the model for one forecast of Hurricane Gilbert (1988). The outermost coarse mesh of 1° resolution, hereafter called mesh C, extending to the boundary of the model domain telescopically contains two meshes M (medium) and F (fine). The mesh M of 1/3° resolution extends 11° in both latitude and longitude. The mesh F of 1/6° resolution covers an area of 5° latitude and longitude. The centers of the inner meshes follow the forecast storm center so that the storm's interior structure is depicted at all times in the finest resolution. Because of the capability of inner mesh relocation, the GFDL hurricane model is called a multiply nested movable mesh (MMM) model. A grid point is placed at the center of each mesh element or box and all meteorological
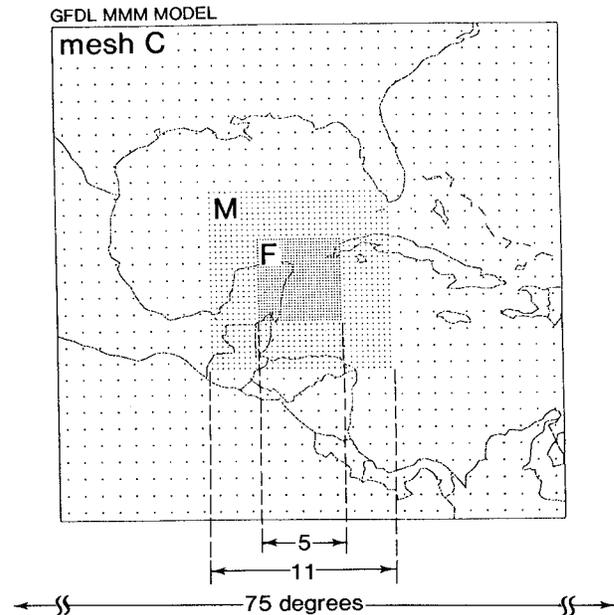
variables are defined there. Use of nonstaggered grids facilitates movement of inner meshes.

In the current prediction system, the mesh nesting is applied to one selected storm at a time. If forecasts are requested for more than one storm, the model is integrated repeatedly with the nested meshes focused on a different storm. For a particular integration, if an additional storm is within the integration domain, that additional storm is resolved only by the coarse outer mesh.

The geographical parameters used in the model, such as the mountain heights and land surface conditions, are prescribed in three datasets containing values at the resolution of meshes C, M, and F, respectively, for the entire global domain. Data sources are the global topography data at 1/6° resolution prepared by the U.S. Navy's Fleet Numerical Oceanography Center and vegetation type data at 1° resolution by Matthews (1983). Topography data for coarser resolution are derived from the average of those in fine subboxes (section 2b of Bender et al. 1987). In case of vegetation-dependent parameters (appendix A of Bender et al. 1993b), a coarse box value is simply assigned to fine subboxes.

c. Finite differencing and a note on pressure gradient calculation

Finite differencing of the governing equations is based on the box method (Kurihara and Holloway 1967). In the computation of fluxes of quantities into or out of a box, values of variables on the sides of the box are needed. These values are obtained from interpolation of grid values. An exception is the estimate of

water vapor mixing ratio at the vertical interface, which uses interpolation of the square root of the mixing ratio in order to reduce the truncation error. If the mixing ratio still takes a negative value at a certain point during the time integration, it is adjusted to a very small positive value by borrowing moisture from each of two levels below.

In the nested mesh configuration, a coarse box at a mesh interface connects to two or more fine boxes. For each segment of an interface, values are obtained by combination of two linear interpolations of grid values, first in the direction parallel to the boundary and, then, in the direction normal to the boundary, (section 2d of Kurihara et al. 1979).

The pressure gradient force at a grid point is estimated from the slope of the isobaric surface that passes through that point. The estimation requires the geopotential heights of the isobaric surface at the lateral sides of the box. How to determine them and the advantage of using the isobaric surface are described in appendix A. No numerical difficulties have been encountered in the computation of the pressure gradient term in the presence of steep terrains.

d. Mesh movement and associated data rearrangement

As mentioned before, the interior meshes F and M are relocated so that their centers are near the forecast storm center at all times (section 2h of Kurihara and Bender 1980). The forecast storm center in the open ocean is determined from the sea surface pressure distribution in the central subdomain of mesh F. Near mountainous terrain, it is determined from the pressure distribution on a horizontal plane that passes the highest peak of the mountains in the subdomain. Specifically, the storm center is the position of the centroid of the negative deviation of the pressure, from an appropriately defined cutoff value, in the central subdomain consisting of 16×16 grid points. Mesh F moves in the zonal and/or meridional direction if the mesh center becomes separated from the forecast storm center by more than one mesh M resolution at the time when meshes F and M are synchronized in the course of model integration (see section 6c). Movement of mesh M depends on an accumulated amount of mesh F movement within mesh M.

When a mesh moves, coarse boxes at the leading edge zone become fine boxes and fine boxes at the trailing edge zone become coarse boxes. First, geographical parameters in the above zones are updated with an appropriate prescribed dataset. Next, meteorological variables as well as the surface height at the new grid point are computed through either interpolation or averaging. The scheme used in this step does not yield fictitious sources of quantities (section 3 of Kurihara et al. 1979). If the computed surface height is different from the prescribed orography data, the prescribed height is adopted. At such a point, the computed values of the temperature and mixing ratio and the surface pressure are adjusted for the difference between the computed and prescribed surface heights and for the resulting sigma-level changes (section 2c of Bender et al. 1987).

4. Model physics

a. Diffusion processes

Effects of horizontal diffusion are estimated by the nonlinear viscosity scheme (Smagorinsky 1963) from the strain due to the resolvable winds for momentum and from the horizontal gradient of the temperature and wind for heat. The diffusion coefficients are determined from the deformation and scale length. For simplicity, the horizontal diffusion is approximated by the diffusion on sigma surfaces.

Effects of vertical diffusion are estimated by the level 2 turbulence closure scheme of Mellor and Yamada (1974, 1982). Vertical diffusion coefficients depend on the vertical shear of the wind, the stability factor using the virtual temperature, and the mixing length. The coefficients obtained above are augmented by background diffusion that is relatively large in the lower levels (section 2a of Kurihara et al. 1990).

b. Similarity theory for surface fluxes

Vertical fluxes of momentum and heat across the ocean and land surface are computed from the friction velocity, friction temperature, and friction mixing ratio of the water vapor. These quantities are obtained in the framework of Monin–Obukhov's similarity theory. In doing so, the diffusive fluxes of momentum and heat are assumed to be constant below the model's lowest level. The wind vanishes at the roughness height. The heat and moisture fluxes below the roughness height—that is, the fluxes in the interfacial layer—are treated with the use of the diffusivity coefficient (section 3b of Kurihara and Tuleya 1974). The input data required are the wind, potential temperature, and water vapor mixing ratio at the lowest level of the model (the wind speed is set to 1 m s^{-1} if it is less than that value), and the potential temperature and saturation mixing ratio at the underlying surface. The surface temperature field at the initial time is provided from a global analysis. The surface temperature is kept unchanged over the ocean, while the land surface temperature after the initial time is predicted.

Universal functions from Hicks (1976) and Carson and Richards (1978) are used to define vertical profiles of momentum, temperature, and moisture above the roughness height. The roughness height over the ocean is related to the friction velocity by Charnock's formula (Wu 1982). Over the land, the roughness height as well as the ground wetness used in the surface moisture specification (section 2b of Tuleya and Kurihara 1978) are prescribed using the vegetation type (appendix A of Bender et al. 1993b).
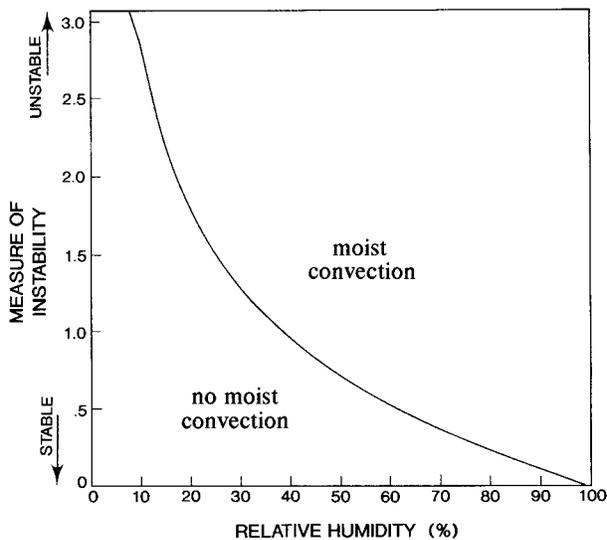
FIG. 2. Condition of the air for free moist convection. A measure of instability—that is, a nondimensional quantity as expressed by the left-hand side of Eq. (B2)—is taken in the ordinate and the relative humidity in the abscissa. A curve separating the favorable and the unfavorable conditions is drawn.

c. Prediction of land surface temperature

The land surface temperature is predicted by a bulk subsurface layer scheme (section 2a of Tuleya 1994). As presented in section 2, the equation for the land surface temperature is expressed in terms of the net heat flux at the surface, soil heat capacity, and the damping depth. The net surface heat flux consists of emission and influx of radiative energy, and the surface exchange of sensible and latent energy. The damping depth is determined from typical values of a soil heat capacity, thermal conductivity of soil, and a period of thermal forcing at the surface.

d. Soft convective adjustment

At each time step of time integration of the model, temperature and moisture are first predicted without including the condensation process. If a state of supersaturation results, the "large-scale condensation" is carried out that reduces the moisture to a saturation level while the latent heat is released to increase the temperature.

The condition of the air is then checked for possible occurrence of cumulus convection. For this purpose, a cloud element is assumed and its buoyancy is examined (Kurihara 1973; appendix C of Kurihara and Bender 1980). It is presumed that the radius of the cloud element depends on the relative humidity of the air surrounding the cloud and the cloud buoyancy is affected by the entrainment of the air into the cloud. The criterion for the occurrence of moist convection is schematically shown in Fig. 2, in which the instability measure and the relative humidity are taken in the ordinate and ab-

scissa, respectively (appendix B). The region above the curve in the figure represents conditions of the air favorable for free moist convection. It indicates that the more unstable the atmosphere is, the lower is the threshold relative humidity for the free moist convection to develop. Accordingly, cumulus convection takes place even at rather low relative humidity if the atmosphere is very unstable, while it does not occur even at high humidity if the stratification is very stable.

If a state of the atmosphere is favorable for moist convection, the scheme initiates the "convective adjustment" in the air column. Suppose that a layer between two adjacent levels is unstable. The scheme makes estimates of the heat budget that is required to make the layer neutral for convection. Collective effects of such estimates in the vertical determine new vertical profiles of temperature and moisture. The new profile is reexamined for further possibility of convection and the iteration proceeds until the entire air column becomes unfavorable for moist convection. In general, the atmosphere thus stabilized is less stable than the atmosphere with the moist-adiabatic lapse rate because of the entrainment effect. Finally, the adjusted profiles of the temperature and the moisture are defined by relaxing the neutralized profile obtained above toward the initial one (appendix B). Owing to the inclusion of the entrainment effect and the relaxation factor in the scheme, the moist convective adjustment performed in the present model is "soft" and appears generally smooth both in time and over the range of spatial resolutions of the triply nested meshes.

e. Radiation effects

Radiation effects are evaluated by the Schwarzkopf and Fels (1991) infrared and Lacis and Hansen (1974) solar radiation parameterizations, including diurnal variation and interactive effects of clouds. Calculated radiative fluxes are updated every 10 min. Clouds are specified where the model condensation takes place.

5. Construction of initial conditions

Initial conditions for the MMM model rely on both the global analysis performed at NCEP and the information on the tropical cyclone structure prepared at the NHC. The former is used to specify the environmental fields as defined below. The latter is utilized in the generation of the tropical cyclone vortex, a key step in the MMM model initialization. In addition, forecasts from the NCEP global model are also obtained to specify the time-dependent lateral boundary conditions for the MMM model.

a. Import of analysis data

Meteorological conditions as well as surface conditions that are globally analyzed at NCEP for a specified

initial time are transferred onto the MMM model grids through spatial interpolation. Imported data are then adjusted for differences in heights of mountains and sigma levels between the global model and the hurricane model. The resulting fields define the analysis fields in the MMM model.

b. Strategy of model initialization

A tropical cyclone analyzed in the NCEP global analysis tends to be too large and too weak because of the limitation in the horizontal resolution. In contrast, the fine mesh of the MMM model is capable of representing tropical cyclone vortices more realistically. Therefore, the model initialization method is formulated using a vortex replacement strategy. Schematically, it is expressed by

initial field

= global analysis − globally analyzed NCEP vortex

+ specified GFDL vortex.

An advantage of the above method is its capability of placing a specified vortex at the observed storm position. A specified vortex is generated at each initial time by using information on the observed storm structure. As mentioned before, to predict more than one storm, the model integration is repeated with the focus put on one selected storm at a time. Only the selected vortex is replaced by the initialization method. Details of the schemes used for vortex replacement are described in Kurihara et al. (1993a), with the upgraded scheme summarized in Kurihara et al. (1995).

c. Environmental field

Removal of the analyzed NCEP vortex is performed in two steps. First, the global analysis is split into two fields through repeated use of a spacial three-point filter to the analysis field,

global analysis = basic field + disturbance field.

The disturbance field is considered as consisting of two components,

disturbance field = globally analyzed NCEP vortex

+ nonhurricane component.

The analyzed NCEP vortex is assumed to be confined within a finite filter domain, whereas the nonhurricane component of the disturbance field has significant magnitude within as well as outside this domain boundary.

In the second step, the nonhurricane component is determined. This is achieved by defining a filter domain that contains the entire analyzed vortex and, then, obtaining the nonhurricane component within that domain. The filter domain is determined by carefully examining the distribution of the low-level disturbance wind in the vicinity of the observed storm. The filter domain is not necessarily circular so that the nearby nonhurricane disturbances are retained. On the boundary of the filter domain and beyond, the disturbance field is assumed to consist entirely of the nonhurricane component. The nonhurricane component within the filter domain is obtained by an optimum interpolation technique using the nonhurricane values provided at the boundary of the filter domain.

Finally, the nonhurricane component is added back onto the basic field to yield the environmental field,

environmental field
= basic field + nonhurricane component.

It is clear that the environmental field thus obtained is identical to the original global analysis except within the filter domain where the ''analyzed NCEP vortex'' is effectively removed.

d. Controlled spinup of a vortex

Generation of a vortex by the method of controlled spinup requires the specification of a target wind field and the time integration of the equations governing the vortex. In the present operational system, an axisymmetric vortex is generated for simplicity using an axisymmetric version of the hurricane prediction model. The hurricane message from the NHC containing data on the wind distribution, size, and height of the storm is exclusively used to define the radial and vertical profiles of the azimuthally averaged tangential wind of the storm. The wind field thus obtained, which will be called the target wind field, controls the tangential winds of the vortex that develops in the model. Specifically, in the course of the time integration, which starts from a calm condition, the tangential winds in the free atmosphere are nudged toward a time-dependent reference wind field. The reference wind field gradually approaches the target field in a long timescale of vortex evolution—for example, 60 h—while nudging is performed using damping timescales that depend on the grid position relative to the storm center. With a shorter damping time, the wind nudging to the reference wind is stronger. The damping timescale is specified so as to yield strong nudging near the storm center in the lower free atmosphere, very weak nudging at higher levels and at large radii, and no nudging in the planetary boundary layer. All fields other than the tangential wind are obtained without constraint during the axisymmetric integration. Consistent with the forecast procedure of the current operational system, the above scheme of vortex generation is applied to one selected storm in each forecast case.

Using a version of the prediction model for the vortex generation guarantees that the initial vortex in the model is more or less consistent with the resolution, physics, and computational schemes used in the forecast model. In addition, unlike a free vortex spinup—that is, a spin-

up without constraint—the above type of controlled spi-nup can generate a vortex that is realistic to a first order in the wind structure and the radial and vertical extent (e.g., Figs. 3 and 5 of Kurihara et al. 1993a; Fig. 1 of Bender et al. 1993b; Fig. 3 of Kurihara et al. 1993b).

After the symmetric vortex is generated, its radial profile of the low-level tangential wind is used in the time integration of a simplified barotropic vorticity equation to estimate the asymmetric wind component due to the beta gyres—that is, a pair of vortices induced by the advection of the planetary vorticity by the symmetric flow (Ross and Kurihara 1992). The combination of the symmetric and asymmetric winds determines the wind of the specified vortex. The mass and moisture fields of the specified vortex are defined by the deviation of these fields in the generated symmetric vortex from the background state.

e. Readjustment of mass fields

The specified GFDL vortex is added to the environmental field with the vortex center placed at the observed location. The resultant wind field provides the wind condition at the initial time. Then, in order to minimize imbalance between the wind and mass fields, the surface pressure field as well as the temperature in the free atmosphere are recomputed by solving a form of the reverse balance equation. This form of the reverse balance equation includes all terms in the divergence equation with the time tendency term bounded by the advection of divergence by the deep layer mean wind—that is, a slow tendency.

6. Time integration scheme

a. Two-step iterative time integration scheme

The MMM model 72-h forecast is performed with a two-step iterative time integration scheme consisting of the predictor step and the corrector step. Although a two-step scheme is less economical than a one-step marching scheme, it is employed to take advantage of its frequency-selective damping characteristics (Kurihara and Tripoli 1976).

In the MMM model, high-frequency gravity waves can be excited due to mesh nesting and particularly due to mesh movement. The two-step scheme is able to keep the fast oscillatory modes from developing in the model without suppressing slow modes. In the application of the two-step scheme to the MMM model, terms in each governing equation are arranged into the slow mode group, fast mode group, and other terms. In a marching process, the slow mode and the fast mode groups are treated using different values for the weight parameter that controls the degree of amplitude damping (appendix C).

TABLE 2. The framework of the GFDL hurricane prediction model.

1) Primitive equation model
2) 18 vertical σ levels
3) Multiply nested movable mesh (MMM)

Mesh	Resolution (°)	Size (°)	Size (points)	Time step (s)
1: coarse	1	75	(75 × 75)	90
2: medium	1/3	11	(33 × 33)	30
3: fine	1/6	5	(30 × 30)	15

4) Physics
   ● Diffusion
       Horizontal: Smagorinsky nonlinear viscosity
       Vertical: Mellor–Yamada turbulence closure scheme level 2 background mixing added
   ● Surface flux
       Monin–Obukhov framework, interfacial layer included
       Ocean: SST (unchanged from the initial field)
       Land: Land surface temperature prediction
           Vegetation type–dependent roughness and wetness
   ● Cumulus convection
       Soft moist-convective adjustment scheme
       entrainment effect considered, relaxation time assumed
   ● Radiation
       Infrared: Schwarzkopf–Fels scheme; solar: Lacis–Hansen scheme
       Effects of diurnal cycle and cloud variation considered
5) Initialization
   Environmental fields from an NCEP global analysis
   Generation of a hurricane vortex by controlled spinup
   Replacement of an NCEP analyzed vortex by the generated vortex
6) Time integration
   Two-step iterative integration scheme
   Wind direction–dependent boundary condition for limited domain
   Mesh-by-mesh integration using dynamical interface

b. Smoothing–desmoothing

Stationary computational noise should not be allowed to develop in the course of a time integration. If not suppressed, these noise features tend to appear in the form of a zigzag or checkerboard pattern. Therefore, a simple smoother is occasionally used to remove the grid-scale variation in the model fields. Immediately following the smoothing, a simple desmoothing operator is used to restore the amplitudes of slow-moving short waves that are undesirably reduced by the smoothing operator (appendix B of Bender et al. 1993b).

c. Dynamical interface

The time integration of the MMM model is performed mesh by mesh using different time steps for different meshes as listed in Table 2. As schematically shown in Fig. 3, the time marching proceeds inward from the outermost mesh. All meshes are synchronized every one
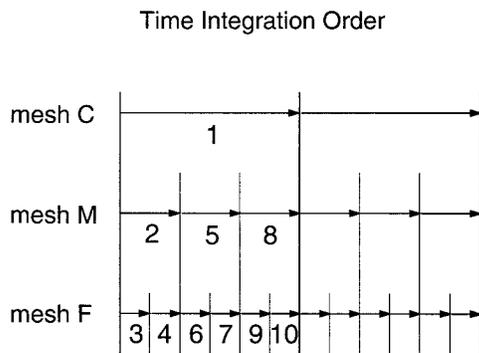
Time Integration Order

FIG. 3. Time integration order of the MMM model. The longest arrow indicates a giant time step.
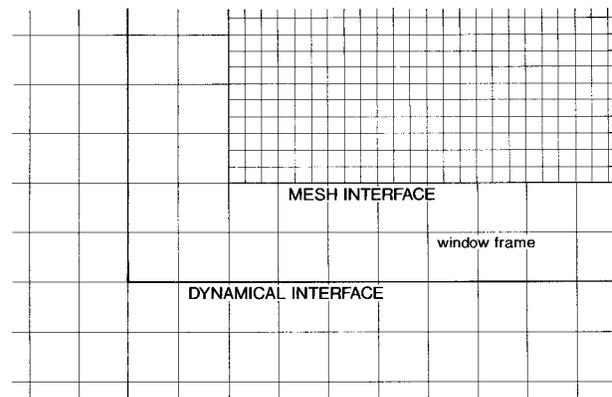

FIG. 4. Position of the dynamical interface. The mesh interface is surrounded by a window frame of two coarse mesh width. The outer rim of the frame is the dynamical interface.

giant time step—that is, at the time levels of mesh C. In between the alignment of all meshes, meshes M and F are aligned two additional times.

Marching of mesh C for one giant time step is carried out using the data in the mesh C domain only. The open lateral boundary conditions are formulated (section 6d) to treat the values in the outermost boundary boxes. On the other hand, since the two-step scheme is used without specifying conditions at the inner boundary, prognosis is not possible for the innermost two grid points. As shown in Fig. 4 a zone containing such points is called the window frame (of an inner mesh). The transport of quantities across the outer rim of the window frame are saved at both the predictor and corrector steps. This information is used when the marching of mesh M is made. In this manner, the window frame region interacts with the region outside of it. Therefore, the outer rim of the window frame is called the dynamical interface.

Marching with mesh M time step is carried out for the region combining the mesh M and the window frame surrounding it. The fluxes that are saved in the mesh C marching are partitioned in time to provide conditions at the dynamical interface (section 2c of Kurihara et al. 1979). In the inner portion of mesh M, fluxes across the outer rim of the window frame of mesh F are saved.

The marching of mesh F is performed for a region consisting of the mesh F domain and its window frame. Fluxes saved in the preceding mesh M marching are used to specify flux conditions at the dynamical interface.

d. Wind direction–dependent open lateral boundary condition

In the mesh C integration, information from the NCEP global forecast is communicated to the outer boundary boxes. Values of these boxes are first predicted by assuming appropriate values at the open side of the boxes. Then, the predicted values are forced toward reference values (Kurihara and Bender 1983; Kurihara et al. 1989). In defining the reference value, the NCEP

forecast at the boundary grid point, its gradient in the direction normal to the boundary, and the MMM predicted values are considered. Because of this, the reference values cannot be prescribed but are obtained in the course of the time integration.

The strength of forcing of the predicted values toward the reference values is dependent on the direction angle of the predicted wind at the boundary grid point relative to the boundary line. The wind direction–dependent scheme yields a gradual change in forcing as the wind direction varies, causing the maximum (minimum) forcing when the predicted wind is normal to the boundary and directed inward (outward). This feature is different from most other schemes in which the forcing depends simply on the direction of the normal component of flow, either inward or outward. The forcing in the planetary boundary layer is reduced to allow the model to establish its own boundary layer structure.

The above forcing scheme generally works in practice with little problem, even in the presence of disturbances near the boundary. However, to suppress the possible appearance of grid-scale variation in the vicinity of the boundary with strong outflow, the above boundary forcing is followed by a smoothing of the wind and moisture fields within a six-gridpoint boundary zone (appendix C of Kurihara and Bender 1980).

7. Performance of the GFDL system in the 1995 hurricane season

a. Framework of the GFDL Hurricane Prediction System

The MMM model is the core of the GFDL Hurricane Prediction System. Its framework is summarized in Table 2. The usage of the model in the prediction system is illustrated in Fig. 5. The system is initiated with a NHC request that specifies which storm to predict and the initial forecast time. Information on the storm structure and position is also supplied from the NHC storm
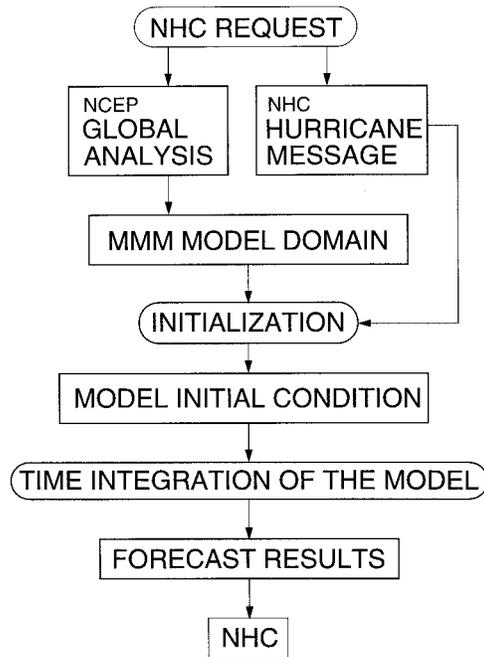
GFDL HURRICANE PREDICTION SYSTEM

FIG. 5. A flowchart of the GFDL Hurricane Prediction System.

TABLE 3. Average track forecast errors (km) in the 1995 hurricane season for the tropical storms and hurricanes in the Atlantic. Statistics are taken for a homogeneous sample of forecasts by GFDL (MMM model), CLIPER (climatology and persistence), BAMD (beta and advection model, deep-layer version), BAMM (medium layer), BAMS (shallow layer), A90E (a statistical–dynamical model), and VBAR (a nested barotropic track forecast model). Errors of OFCL (official forecast) are also listed. The number of cases for each forecast time is shown at the bottom row in parentheses.

Model	Forecast time (h)				
	12	24	36	48	72
GFDL	95	165	218	270	395
CLIPER	100	215	337	452	666
BAMD	97	185	265	333	530
BAMM	105	199	284	356	546
BAMS	121	235	344	430	630
A90E	90	167	253	343	590
VBAR	88	180	269	352	560
OFCL	86	165	236	297	450
Cases	(218)	(209)	(194)	(177)	(146)

message file. The first phase of the system is to interpolate the NCEP global analysis data at the specified time onto grid points of the hurricane model. The global model forecast data are also saved for later use in the prediction phase. In the second phase, the model initial conditions are determined through the method of vortex replacement. In this phase, the storm information is used to generate a spinup vortex. The third phase is to carry out the time integration of the MMM model to make a 72-h prediction. The final phase provides the hurricane forecasters with model-generated guidance products such as a time series of the storm location, minimum pressure, maximum wind, a map of storm track and the maximum wind distribution during the forecast period, maps showing initial wind conditions, and time sequences of various meteorological fields.

b. Performance of the GFDL system: Storm track prediction

Tropical cyclone activity was unusually high in the Atlantic in the 1995 hurricane season. The GFDL system made 257 forecasts for the Atlantic tropical cyclones including depressions as well as 105 forecasts for the eastern Pacific basin.

To evaluate the storm track forecast error, the forecast positions of the storm center as defined in section 3d are compared against the best track positions determined by NHC. Average errors in predicted positions at 24, 48, and 72 h in the Atlantic basin are 164 km (232 cases), 281 km (192 cases), and 400 km (150 cases),

respectively. The corresponding statistics for the eastern Pacific at 24, 48, and 72 h are 138 km (99 cases), 250 km (78 cases), and 324 km (56 cases), respectively. The corresponding errors for the simplest model, CLIPER, which relies on the track climatology and the track persistence, are 204, 433, and 615 km in the Atlantic and 158, 322, and 389 km in the eastern Pacific basin. A conventional score to measure the skill of the model performance is the percentage comparison against CLIPER, that is, [(average position error of the MMM model) − (average position error of CLIPER)]/(average position error of CLIPER). The track forecast skills of the MMM model at 24, 48, and 72 h are −20%, −35%, and −35% in the Atlantic and −13%, −22%, and −17% in the eastern Pacific (note that minus values indicate improvement over CLIPER). The percentage improvement in the eastern Pacific basin is relatively small partly due to the smaller error of CLIPER in that basin compared with the Atlantic.

Average position errors of several models (for homogeneous cases excluding tropical depressions) are presented in Tables 3 and 4 separately for the Atlantic and eastern Pacific. Also listed are the errors for the official forecasts, which were made before many of the model forecasts including GFDL became available. In the Atlantic, the improvement of track forecasts by the MMM model is substantial after 36 h. The improvement relative to the next best model of NWS at 36, 48, and 72 h are 14%, 19%, and 25%, respectively. In the eastern Pacific, the GFDL system is the best performer among the NWS guidance after 24 h. Figure 6 shows how the average track forecast error of each NWS guidance increases with time. It is clearly seen that the rate of error increase with the forecast time of the GFDL model is much less compared with those of other guidance throughout the forecast period. In the Atlantic the GFDL error at 72 h is comparable to the errors at 48 h of other guidance. The slopes of lines in the figure suggest that

TABLE 4. Average track forecast errors (km) in the 1995 hurricane season for the tropical storms and hurricanes in the eastern Pacific. Statistics are taken for a homogeneous sample of forecasts by GFDL (MMM model), CLIPER (climatology and persistence), BAMD (beta and advection model, deep-layer version), BAMM (medium layer), BAMS (shallow layer), PSS (Pacific statistical synoptic model), and P91E (a statistical–dynamical model). Errors of OFCL (official forecast) are also listed. The number of cases for each forecast time is shown at the bottom row in parentheses.

Model	Forecast time (h)				
	12	24	36	48	72
GFDL	81	139	190	248	305
CLIPER	75	158	234	304	420
BAMD	88	158	218	273	321
BAMM	95	179	270	355	437
BAMS	99	194	292	384	526
PSS	74	151	220	285	425
P91E	74	148	208	256	332
OFCL	70	144	211	263	315
Cases	(86)	(76)	(67)	(58)	(37)

increase in the track forecast accuracy shortly after the initial time is needed for improvement of predictions at later times.

Examples of two highly skillful predictions in the Atlantic are presented in Figs. 7 and 8 in which composites of the track predictions starting at 12-h intervals are shown together with the observed storm positions estimated by NHC. In the case of Hurricane Luis, changes in its track including the northward turn are predicted extremely well over the entire life of the storm. As a result, the GFDL model exhibited improvements of about 60% and 70% over CLIPER at 48 and 72 h, respectively. Predictions of Hurricane Marilyn's track generally agree well with observations, with a percentage improvement of about 45% over CLIPER after 48 h. On the other hand, as shown in Fig. 9, the GFDL model exhibits some westward bias in the track prediction for Hurricane Opal. Also, the model storm moves northward too fast. The westward bias is also clearly noticed in cases of Hurricane Roxanne (figure not shown).

It has been suggested from analysis results of the track forecasts in a few recent hurricane seasons that the position error tends to be relatively small in the central region of the Atlantic basin at all forecast times, compared against the prediction errors in the region of the Gulf of Mexico. Shown in Figs. 10 and 11 are the average error distributions and the vector bias, respectively, for the forecast positions at 48 h in the 1995 hurricane season. (The figures are based on a weighted average computed at each 1° grid point for cases in which storm forecast positions were within 10° distance.) Figure 10 confirms that the forecast error at 48 h was relatively small over the central Atlantic, with a minimum of 105 km. The distribution of the CLIPER forecast position error (figure not shown) shows a pattern somewhat similar to that of GFDL in the central Atlantic with a minimum value of 167 km, close to the
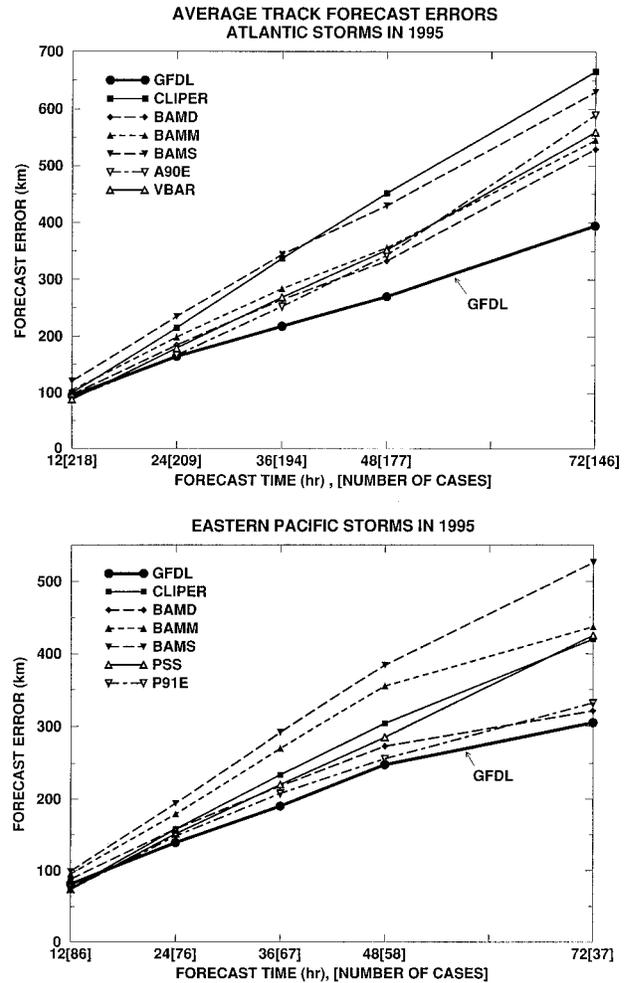

FIG. 6. Average track forecast errors (km) in the 1995 hurricane season for the tropical storms and hurricanes in the Atlantic (upper panel) and in the eastern Pacific (lower panel). Forecast time and number of cases (in brackets) are taken in the abscissa.

minimum value of the GFDL error. When Fig. 10 is compared against the CLIPER error distribution, significant skill of the GFDL model is indicated over most of the Atlantic region. On the other hand, the forecast error in the gulf region is generally large both for GFDL and CLIPER, with northward decrease of error in GFDL and increase in CLIPER. The GFDL model does not show forecast skill over and in the vicinity of the Yucatan peninsula, while some skill exists in the northern part of the gulf. It is evident from Fig. 11 that a large westward bias existed in the Gulf of Mexico region. Large bias both in the gulf and elsewhere is a significant contributor to the total GFDL track error. The Gulf of Mexico region is surrounded by landmasses with high mountains to the west and south. Such features can introduce complexity (baroclinic condition) and inaccuracy in the analysis in the large-scale flow as well as in the specification of the bogus vortices. (According to our evaluation, changes in the global analysis system
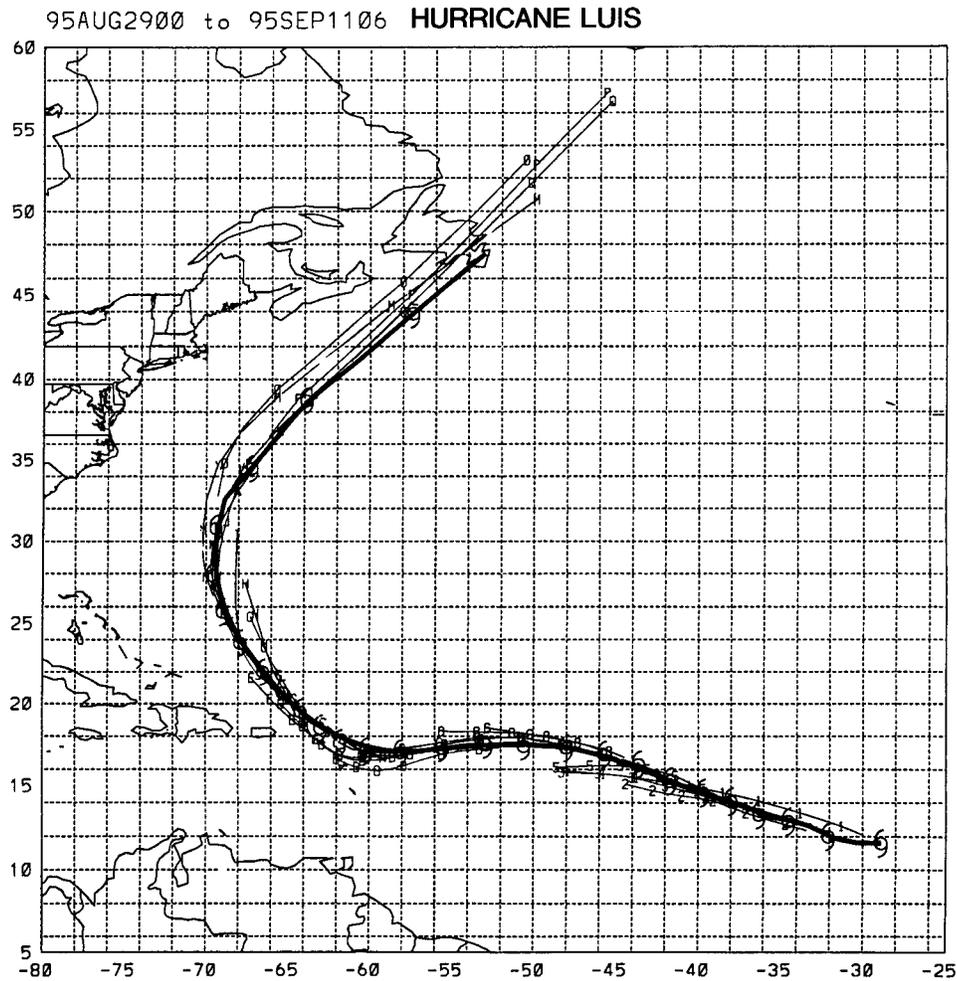
FIG. 7. Composite of track forecasts of Hurricane Luis. Thin lines indicate track predictions started at 12-h intervals. The thick line shows the observed track connecting 12-h positions (storm symbols). Latitude and longitude lines are drawn at the 2° interval.

at NCEP late in 1995 have corrected to some degree the GFDL track forecast bias and errors in the Atlantic basin.) Besides the initial condition problem, better forecast requires the accurate estimate of the interaction between the model vortex and mountains throughout the forecast period. In separate studies (e.g., Bender et al. 1993a), significant impact due to the storm's interaction with the underlying water of the open ocean area was hinted. Such an effect is not considered in the present system but can modify the storm structure and, hence, its movement. This effect may be large in the case of the relatively shallow waters of the Gulf of Mexico.

c. Performance of the GFDL system: Storm intensity prediction

The MMM model is capable of simulating the first-order structure in the interior region of a hurricane vortex. However, the prediction of the tropical cyclone intensity is far from successful. Analysis for the past sev-

eral hurricane seasons indicates that there is a tendency for the maximum wind speed of the storm to be over-predicted in the case of weak storms and underpredicted in the case of strong storms. The cause of the over-prediction of intensity is an important subject for future investigation. The underprediction is likely related to the resolution problem. The treatment of deep convection in the model has to be evaluated from the viewpoint of the intensity forecast. The average errors and the bias of the maximum wind speed prediction by a few methods and the official forecast are listed in Table 5. The GFDL error at 12 h is 6.1 m s^{-1} as compared with 3.1–3.8 m s^{-1} for other guidance. However, the error increase between 24 and 72 h is only 1.8 m s^{-1} in contrast to 3.7–5.1 m s^{-1} for other guidance. This results in superior performance of the GFDL forecast at 72 h in 30% of cases in an ensemble of available guidance, official forecast, and persistence. Note that the intensity error at the initial time is not necessarily zero for the GFDL model, while it is practically zero for the statistical scheme.

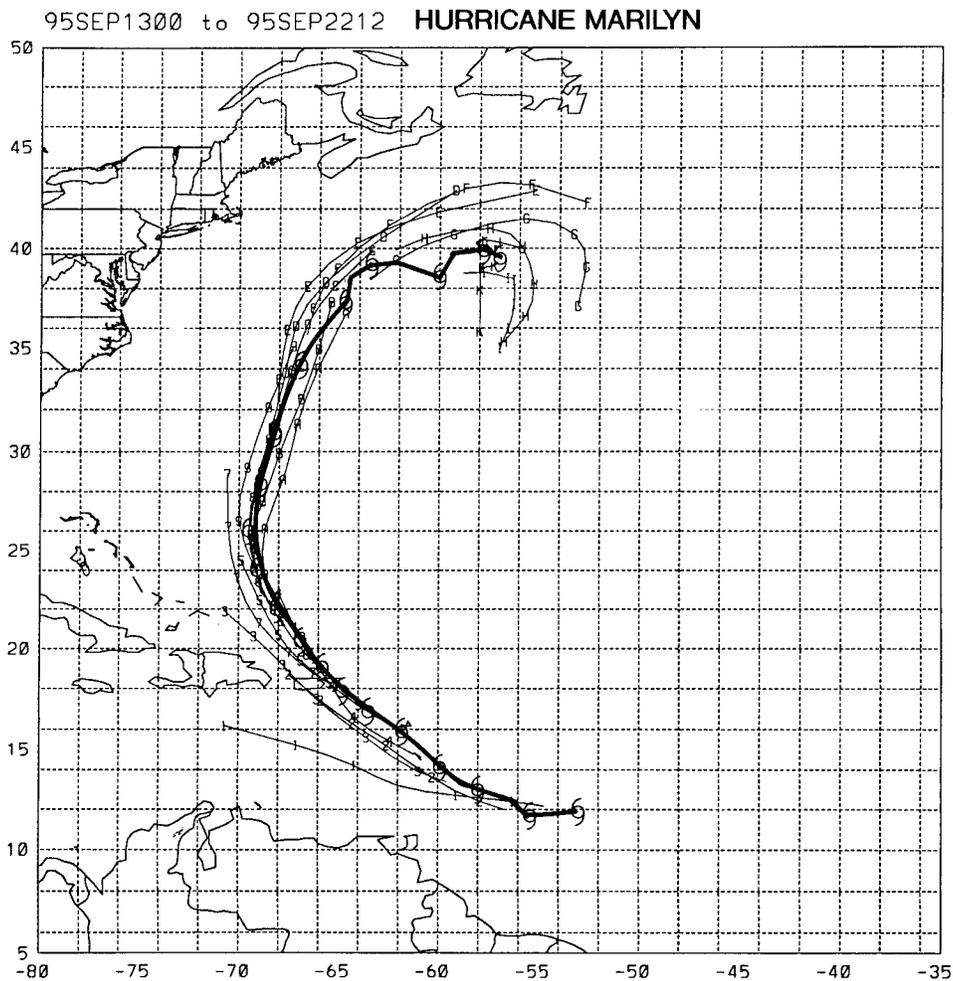95SEP1300 to 95SEP2212 **HURRICANE MARILYN**

FIG. 8. Same as Fig. 7 but for Hurricane Marilyn.

Also, the GFDL storm, which is initially generated in the calm environment through controlled spinup, undergoes a structure change after the start of the model integration. When each of the GFDL forecasts is corrected for the error in the earlier period, the result becomes competitive with other guidances. This correction has become available to the NHC forecasters starting with the 1996 hurricane season. The average intensity bias of the GFDL model is positive at all forecast times, different from other models. The positive bias resulted from a combination of a large number of cases, in which the intensity was overpredicted and a few storms that exhibited very large positive error in the intensity. The error statistics strongly suggest a need for the improvement in the initialization method.

8. Summary and remarks

The framework of the MMM hurricane prediction model constructed at GFDL and the outline of the GFDL Hurricane Prediction System are described in this paper.

Also, the performance of the GFDL system in the 1995 hurricane season is briefly summarized.

Major features of the MMM model include (a) the multiply nested movable mesh configuration, which is capable of depicting the interior structure of tropical cyclones; (b) cumulus parameterization with a soft moist convective adjustment scheme, in which the entrainment effect on a cloud element is considered; (c) the model initialization by the method of vortex replacement, which involves generation of a hurricane vortex through a controlled spinup process using the prediction model; and (d) time integration of the nested model using defined dynamical interfaces and utilizing the selective-damping property of a two-step iterative scheme.

In 1995, the GFDL Hurricane Prediction System was adopted by the NWS as an official forecast tool for tropical cyclone prediction. In both the Atlantic and eastern Pacific basins, the storm track prediction in 1995 showed substantial improvement compared with predictions from several other models, in particular in the forecast period beyond 36 h. For example, improve-

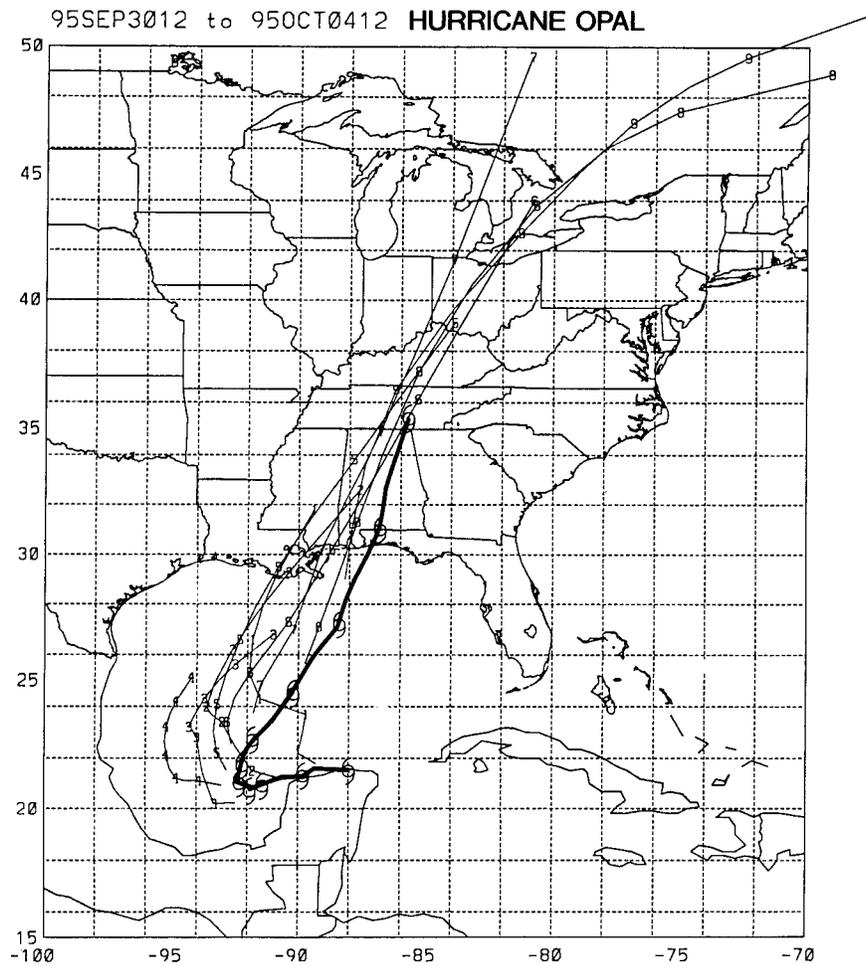95SEP3012 to 950CT0412 **HURRICANE OPAL**
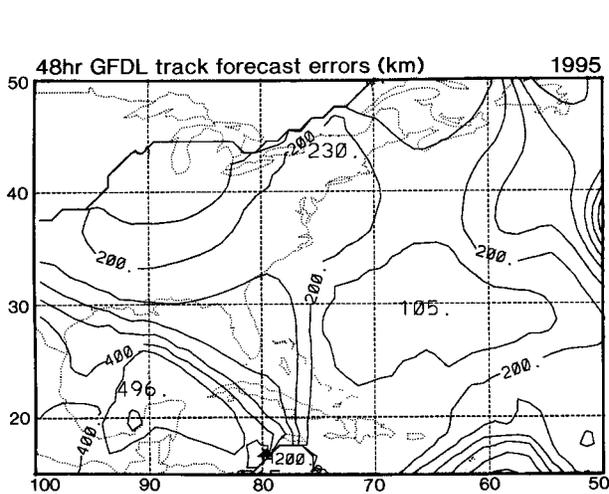

FIG. 9. Same as Fig. 7 but for Hurricane Opal.

FIG. 10. Distribution of the average track forecast errors (km) by the GFDL model at 48-h forecast time in the Atlantic basin during the 1995 hurricane season. The contour interval is 50 km.
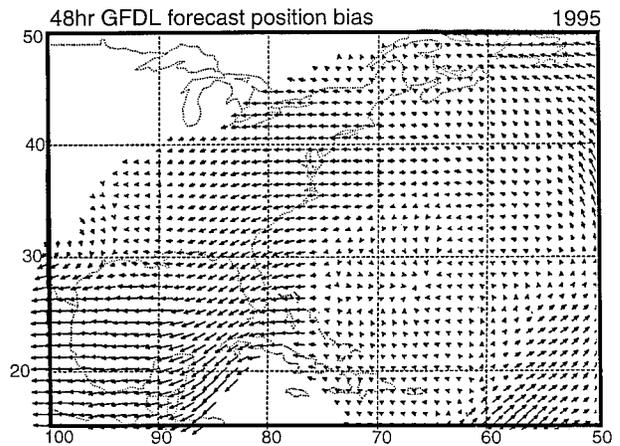

FIG. 11. Distribution of the bias of the storm track forecast by the GFDL model at 48-h forecast time in the Atlantic basin in the 1995 hurricane season. The head of the arrow represents the forecast position and the tail the observed position. Accordingly, the arrow indicates the forecast bias.

TABLE 5. Average forecast errors of the maximum surface wind (m s^{-1}) and the forecast bias (in parentheses, m s^{-1}) in the 1995 hurricane season for the tropical storms and hurricanes in the Atlantic. Statistics are taken for a homogeneous sample of forecasts by GFDL (MMM model), NCHG (persistence), SHIFOR (Statistical Hurricane Intensity Forecast), and SHIPS (Statistical Hurricane Intensity Prediction Scheme). Errors of OFCL (official forecast) are also listed. The number of cases for each forecast time is shown at the bottom row in parentheses.

Model	Forecast time (h)				
	12	24	36	48	72
GFDL	6.1 (0.3)	7.9 (2.3)	8.3 (3.5)	8.4 (4.1)	9.7 (5.0)
NCHG	3.3 (−0.5)	5.5 (−0.9)	7.2 (−0.8)	8.8 (−0.9)	10.6 (−1.3)
SHIFOR	3.8 (−0.1)	5.0 (−0.4)	6.2 (−0.5)	7.5 (−0.6)	8.7 (−1.8)
SHIPS	3.8 (−0.4)	5.0 (−0.9)	6.2 (−2.0)	7.7 (−3.2)	8.7 (−6.0)
OFCL	3.1 (0.0)	4.6 (−0.2)	5.7 (−0.3)	7.4 (−1.0)	9.0 (−0.3)
Cases	(218)	(210)	(197)	(177)	(142)

ments in the track forecasts in the Atlantic at 36, 48, and 72 h are 14%, 19%, and 25%, respectively, relative to the next best NWS guidance at each forecast time. The GFDL model possesses an advantage over the other models since its nested fine mesh better resolves the compact three-dimensional structure of a tropical cyclone at the initial time and throughout the forecasting period. It is likely that this makes simulation of the vortex–environment interaction more realistic.

Case-by-case evaluation of the performance as well as the distributions of the forecast error and bias suggest that tropical cyclone track prediction in the Gulf of Mexico is more difficult than that in the middle Atlantic. In general, an accurate prediction of the initial movement of a storm is needed for an accurate track prediction at later times. The model performance in the forecast of storm intensity is not yet at a satisfactory level. However, a hint of skill shown at later forecast periods is encouraging.

It should be always remembered that, although the statistical results are supposed to be a measure of overall performance of the model, the results are sensitive to the presence of a small number of abnormal cases. Also, the statistical results obtained for one particular year may or may not be valid in another year. This is because sensitivity of the model behavior to the interannual variation of the environmental conditions cannot be assessed from the model performance in just one year. In the case of the GFDL prediction system, its remarkable performance has been demonstrated in each of the Atlantic hurricane seasons from 1993 through 1996.

Guided by the postseason analysis of the track predictions in 1995 and extensive tests, two changes were implemented in the system in 1996. First, the radius of the specified vortex in the initial condition is now limited to 1000 km. In the previous version, this was simply chosen as twice the radius of the outermost closed isobar with no upper limit on storm size. Tests using the above change resulted in a 10%–15% percent reduction in the average track error in the first 24-h period in 20 forecasts of two large hurricanes, Hurricanes Felix and Opal.

The other change concerns the smoothing of fields in

the six gridpoint zone made after the open lateral boundary forcing (section 6d). The smoothing weights used for the first to sixth grid points are now a function of the wind angle, relative to the boundary line, at the first point and are slightly increased in cases of outflow. The weights previously used were not sufficient for noise suppression in some cases of very strong outflow.

The MMM hurricane prediction system was also applied in test mode in 1995 to forecast typhoons in the western Pacific basin. The system produced accurate track predictions in many cases and the extensive performance evaluation will be made in a separate paper. As a result, the U.S. Navy has adopted the GFDL prediction system and combined it with their global analysis data to use as an official tool for typhoon prediction starting in 1996.

The performance of the prediction system can be improved further. Above all, the initial condition of the model should be made more accurate. This requires a higher quality global analysis on the one hand, possibly by utilizing observational data that are already available or obtainable in the future. On the other hand, the scheme of controlled spinup of the hurricane vortex should be improved. For example, the influence of environmental winds should be taken into consideration in the process of vortex generation. This can be an intermediate step to the four-dimensional data assimilation approach. Upgrading of the model physics, in particular the cumulus parameterization scheme, is a key research area for prediction improvement, particularly for hurricane intensity prediction. Inclusion of the hurricane–ocean interaction process with the use of a hurricane–ocean coupled model is needed to improve the skill of the model's intensity forecasts. Experimental tests using a coupled model are planned for the 1997 hurricane season.

GFDL director, and J. Mahlman, GFDL director, during the very long course of the present study. We also appreciate the strong support and encouragement of R. McPherson, E. Kalnay, S. Lord, R. Sheets, and R. Burpee in the operational implementation of the GFDL Prediction System. We thank T. Knutson and C.-C. Wu for valuable comments on the manuscript, the referees for comments and suggestions, and K. Raphael and J. Varanyak for assistance with figure preparation.

Slope of an Isobaric Surface in the σ Coordinate

In the GFDL hurricane model, the pressure gradient force is determined from the slope of an isobaric surface. Consider the isobaric surface passing point A in Fig. A1. Its gradient can be estimated if the height of point B where that surface intersects a vertical line at distance d is known. If the pressure at the ground surface G is greater than the pressure at A as in Fig. A1a in the figure, point B is above point G and can be located in between σ surfaces C and D. The height of B can be computed from the known heights of C and D by appropriate interpolation. If the surface pressure at G is less than

the pressure at A, point B is below the ground surface (Fig. A1b). The depth of a fictitious air column between G and B in hydrostatic balance is then estimated. In this computation, the average of temperatures at A and F (the lowest model level) is taken for the mean temperature in the column. In the conventional scheme used in the σ-coordinate system, the pressure gradient is obtained from the combination of two terms. Schematically, one term determines the height of point E and the other term attempts to estimate the height difference between E and B. In the computation of the latter term, the temperature at A and/or E, not those between E and B, is used. Such a computation can cause inaccuracy in the estimate of the pressure gradient force.

Criterion for Free Moist Convection and Adjustment of the Temperature and Moisture Profiles

In general, two issues are posed in the formulation of a convective adjustment scheme: (a) the condition for the free moist convection to occur, and (b) the state to which the temperature and moisture is adjusted. In the GFDL hurricane model, a cloud element is used to deal with these problems (Kurihara 1973). The buoyancy of the cloud element is affected by entrainment of the air.

Expressing the rate of entrainment of the air by E, the condition for free moist convection is written,

$$-\frac{\partial T}{\partial z} - \gamma_m - H(r_s - r)E > 0, \qquad \text{(B1)}$$

where γ_m is the moist-adiabatic lapse rate, r_s the saturation mixing ratio and, using conventional notations, $H = L[c_p + (L\varepsilon/p)(de_s/dT)]^{-1}$. Let D denote the radius of the cloud element. It is assumed that D is a function of the relative humidity: $D = D_0 h^{1/2}$, where h is the relative humidity (normalized by 100%; $0 \leq h \leq 1$). The quantity D_0, which represents the cloud radius at $h = 1$ is disposable. The value of D_0 currently used is 500 m above the level $\sigma = 0.918$ ($\sim$700 m), linearly decreasing to 0 at $\sigma = 1.0$. Therefore, no clouds exist at the ground surface at all times and, also, in the completely dry environment. The rate of entrainment E is given by an empirical formula: $E = 0.2/D$. Using E thus defined, (B1) becomes

$$\left(-\frac{\partial T}{\partial z} - \gamma_m\right)\frac{D_0}{0.2Hr_s} > (1 - h)h^{-1/2}. \qquad \text{(B2)}$$

The left-hand side of the above inequality formula is a nondimensional quantity representing a measure of moist convective instability. Larger lapse rate $-\partial T/\partial z$ and larger D_0 yield larger instability. Given the instability measure, the relative humidity has to be larger than a threshold value for free moist convection to occur.
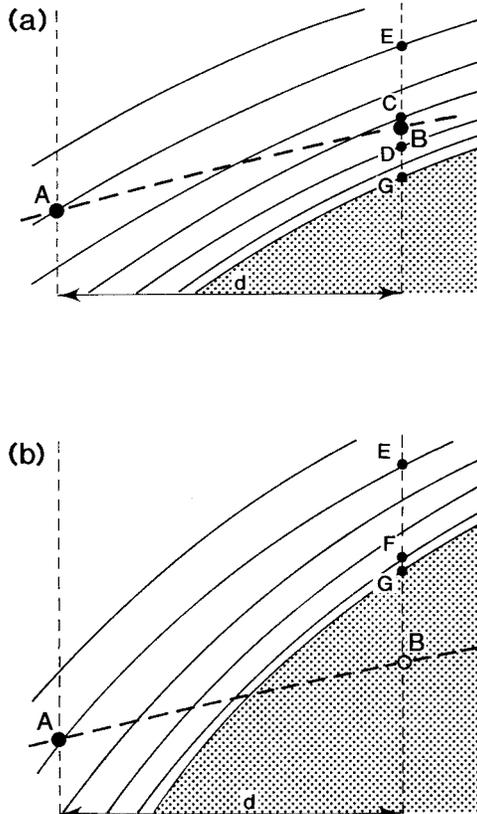
FIG. A1. Position of points in the vertical cross section. Shaded region represents a land mass. Closed circles in both (a) and (b) are located in the air and an open circle in (b) is below the ground surface. The dashed line AB indicates an isobaric surface.

On the other hand, given the relative humidity, the instability measure has to be larger than a certain threshold value. Such a condition is illustrated in Fig. 2. For $p = 1000$ hPa, $T = 298$ K, and $-\partial T/\partial z = 0.65$ K/100 m, the instability measure is $1.05 \times 10^{-3}D_0$ (where D_0 is in meters). It becomes 0.525 for $D_0 = 500$ m. The threshold relative humidity for this instability is about 60% and the cloud radius corresponding to it is approximately 390 m. Due to the relation assumed between D and D_0, (B2) is rewritten as

$$D > 0.2Hr_s\left(-\frac{\partial T}{\partial z} - \gamma_m\right)^{-1}(1 - h). \quad \text{(B3)}$$

The above formula indicates that the radius of the cloud element is larger than the value of the right-hand side of (B3). For the same values of p, T, and $-\partial T/\partial z$ as specified above, the cutoff radius is 381, 286, and 190 m in an environment of 60%, 70%, and 80% relative humidity, respectively.

If the state of the air is favorable for occurrence of free moist convection, the effects of cumulus convection are supposed to stabilize the state. The neutralized state is expressed by changing the inequality sign in the above convection criterion to the equality sign. Suppose that a state of a layer between two adjacent levels is unstable. Then, the amount of heat attributable to the latent heat release and its partition to the two levels that are required to stabilize the layer are computed (Kurihara 1973). The collection of effects thus computed separately for each originally unstable layer yields modified profiles of T and r. The new sounding is examined for possible further modification. Such iteration proceeds until the entire air column becomes stable.

In the MMM model, the temperature and the moisture profiles are adjusted to a state in between the above obtained stable profile and the original profile. Specifically, the difference between the two profiles is multiplied by a reduction factor—that is, the time step in use divided by a relaxation time (5 min)—to determine the amount of adjustment done for that time step.

APPENDIX C

Two-Step Time Integration Scheme

Governing primitive equations presented in section 2 are written in the following symbolic form, in which h represents a time-dependent variable: $h = u,\ v,\ T,\ r$,

$$\frac{\partial p_* h}{\partial t} = \text{LF} + \text{HF} + \text{DF} + \text{AD}.$$

In the above, LF and HF are called the low-frequency and high-frequency terms, respectively; DF the diffusion terms; and AD the forcing terms (effects of condensation, convection, radiation). Specifically,

$$\text{LF} = -\nabla \cdot (p_* h\mathbf{v}) - \frac{\partial}{\partial \sigma}(p_* h\dot{\sigma}) - h\frac{\partial p_*}{\partial t},$$

$$\text{HF} = h\frac{\partial p_*}{\partial t} + \text{(Coriolis force, metric force,}$$

pressure gradient force for $h = u,\ v$;
energy conversion terms for $h = T$),

DF = (effects of horizontal and vertical diffusion),
AD = (moist convection + radiation for $h = T$;
moist convection for $h = r$).

Note that the right-hand side of the surface pressure tendency equation belongs to HF.

To advance a variable h by a time increment Δt from a time level τ to $\tau + 1$, a tentative value h^* is obtained in the predictor step:

$$h^* = h^\tau + (\text{LF}^\tau + \text{HF}^\tau + \text{DF}^\tau)\Delta t,$$

where LF^τ, etc., mean that these terms are computed from variables at the time level τ. Let LF^*, etc., denote these terms computed from the tentative values h^*. In the corrector step, $h^{\tau+1}$ is obtained by first computing

$$h^{\tau+1} = h^\tau + [(1 - \alpha)\,\text{LF}^\tau + \alpha\,\text{LF}^*]$$
$$+ [(1 - \beta)\,\text{HF}^\tau + \beta\,\text{HF}^*]$$

and next adding the forcing effect $\text{AD}^{\tau+1}$ to the above. Values assigned to the weight parameters α and β in the above equation are 0.506 and 2.5, respectively, with some exceptions (section 2e of Kurihara and Bender 1980). Using these weights, the low-frequency waves are preserved in time marching, whereas the amplitudes of the high-frequency waves are strongly suppressed.

REFERENCES

Bender, M. A., R. E. Tuleya, and Y. Kurihara, 1987: A numerical study of the effect of island terrain on tropical cyclones. *Mon. Wea. Rev.,* **115,** 130–155.
——, I. Ginis, and Y. Kurihara, 1993a: Numerical simulations of tropical cyclone-ocean interaction with a high-resolution coupled model. *J. Geophys. Res.,* **98,** 23 245–23 263.
——, R. J. Ross, R. E. Tuleya, and Y. Kurihara, 1993b: Improvements in tropical cyclone track and intensity forecasts using the GFDL initialization system. *Mon. Wea. Rev.,* **121,** 2046–2061.
Carson, D. J., and P. J. R. Richards, 1978: Modelling surface turbulent fluxes in stable conditions. *Bound.-Layer Meteor.,* **14,** 67–81.
Hicks, B. B., 1976: Wind profile relationships from the ''Wangala'' experiment. *Quart. J. Roy. Meteor. Soc.,* **102,** 535–551.
Kanamitsu, M., 1989: Description of the NMC global data assimilation and forecast system. *Wea. Forecasting,* **4,** 335–342.
——, and Coauthors, 1991: Recent changes implemented into the global forecast system at NMC. *Wea. Forecasting,* **6,** 424–435.
Kurihara, Y., 1973: A scheme of moist convective adjustment. *Mon. Wea. Rev.,* **101,** 547–553.
——, and J. L. Holloway, 1967: Numerical integration of a nine-level global primitive equations model formulated by the box method. *Mon. Wea. Rev.,* **95,** 509–530.
——, and R. E. Tuleya, 1974: Structure of a tropical cyclone developed in a three-dimensional numerical simulation model. *J. Atmos. Sci.,* **31,** 893–919.
——, and G. J. Tripoli, 1976: An iterative time integration scheme designed to preserve a low-frequency wave. *Mon. Wea. Rev.,* **104,** 761–764.
——, and M. A. Bender, 1980: Use of a movable nested-mesh model for tracking a small vortex. *Mon. Wea. Rev.,* **108,** 1792–1809.
——, and ——, 1983: A numerical scheme to treat the open lateral

boundary of a limited area model. *Mon. Wea. Rev.,* **111,** 445–454.

——, G. J. Tripoli, and M. A. Bender, 1979: Design of a movable nested-mesh primitive equation model. *Mon. Wea. Rev.,* **107,** 239–249.

——, C. L. Kerr, and M. A. Bender, 1989: An improved numerical scheme to treat the open lateral boundary of a regional model. *Mon. Wea. Rev.,* **117,** 2714–2722.

——, M. A. Bender, R. E. Tuleya, and R. J. Ross, 1990: Prediction experiments of Hurricane Gloria (1985) using a multiply nested movable mesh model. *Mon. Wea. Rev.,* **118,** 2185–2198.

——, ——, and R. J. Ross, 1993a: An initialization scheme of hurricane models by vortex specification. *Mon. Wea. Rev.,* **121,** 2030–2045.

——, R. E. Tuleya, M. A. Bender, and R. J. Ross, 1993b: Advanced modeling of tropical cyclones. *Tropical Cyclones Disasters,* J. Lighthill et al., Eds., Peking University Press, 190–201.

——, M. A. Bender, R. E. Tuleya, and R. J. Ross, 1995: Improvements in the GFDL hurricane prediction system. *Mon. Wea. Rev.,* **123,** 2791–2801.

Lacis, A. A., and J. E. Hansen, 1974: A parameterization for the absorption of solar radiation in the earth's atmosphere. *J. Atmos. Sci.,* **31,** 118–133.

Lord, S. J., 1991: A bogusing system for vortex circulations in the National Meteorological Center global forecast model. Preprints, *19th Conf. on Hurricanes and Tropical Meteorology,* San Antonio, TX, Amer. Meteor. Soc., 328–330.

Matthews, E., 1983: Global vegetation and land use: New high-res-olution data bases for climate studies. *J. Climate Appl. Meteor.,* **22,** 474–487.

Mellor, G. L., and T. Yamada, 1974: A hierarchy of turbulence closure models for planetary boundary layers. *J. Atmos. Sci.,* **31,** 1791–1806.

——, and ——, 1982: Development of a turbulence closure model for geophysical fluid problems. *Rev. Geophys. Space Phys.,* **20,** 851–875.

Parrish, D. H., and J. C. Derber, 1992: The National Meteorological Center's spectral statistical-interpolation analysis system. *Mon. Wea. Rev.,* **120,** 1747–1763.

Ross, R. J., and Y. Kurihara, 1992: A simplified scheme to simulate asymmetries due to the beta effect in barotropic vortices. *J. Atmos. Sci.,* **49,** 1620–1628.

Schwarzkopf, M. D., and S. B. Fels, 1991: The simplified exchange method revisited: An accurate, rapid method for computation of infrared cooling rates and fluxes. *J. Geophys. Res.,* **96,** 9075–9096.

Smagorinsky, J., 1963: General circulation experiments with the primitive equations. Part I: The basic experiment. *Mon. Wea. Rev.,* **91,** 99–164.

Tuleya, R. E., 1994: Tropical storm development and decay: Sensitivity to surface boundary conditions. *Mon. Wea. Rev.,* **122,** 291–304.

——, and Y. Kurihara, 1978: A numerical simulation of the landfall of tropical cyclones. *J. Atmos. Sci.,* **35,** 242–257.

Wu, J., 1982: Wind-stress coefficients over sea surface from breeze to hurricane. *J. Geophys. Res.,* **87,** 9704–9706.